Eye Histology and Ganglion Cell Topography of Northern Elephant Seals (*Mirounga angustirostris*)

HRVOJE SMODLAKA,[1]* WAEL A. KHAMAS,[1] LAUREN PALMER,[2] BRYAN LUI,[1] JOSIP A. BOROVAC,[3] BRIAN A. COHN,[4] AND LARS SCHMITZ[4]

[1]College of Veterinary Medicine, Western University of Health Sciences, Pomona, California

[2]The Marine Mammal Care Center at Fort MacArthur, San Pedro, California

[3]School of Medicine, University of Split, Split, 21000, Croatia

[4]Claremont McKenna, Pitzer and Scripps Colleges, W.M. Keck Science Department Claremont, California

ABSTRACT

Northern elephant seals are one of the deepest diving marine mammals. As northern elephant seals often reach the bathypelagic zone, it is usually assumed that their eyes possess evolutionary adaptations that provide better ability to see in dim or scotopic environments. The purpose of this study was to carefully describe anatomical and histological traits of the eye that may improve light sensitivity. Northern elephant seals have large, somewhat elliptical eyes, with equatorial and anteroposterior diameters of 5.03 and 4.4 cm, respectively. The cornea is large in diameter and the lens is completely spherical. The iris has pronounced constrictor and dilator muscles, whereas the ciliary muscle is notably less developed. The tapetum lucidum is more prominent than in other pinnipeds, making up about 63% of retinal thickness in the posterior aspect of the globe. Within the retina, the pigmented epithelium lacks pigment except for the region close to the ora serrata. Parts of the photoreceptor and outer nuclear layers are folded. Although the photoreceptor layer is composed predominantly of rods, cone photoreceptors were also observed. Cells within the retinal ganglion cell layer are arranged in a single level. Ganglion cells reach their maximum density ($\sim$1,300 cells per mm^2) dorsal to the optic disc, whereas the periphery of the retina is sparsely populated ($<$100 cells per mm^2). All above mentioned features are consistent with the predicted evolutionary adaptations to the photic environment of the bathypelagic zone. Anat Rec, 299:798–805, 2016.

Key words: eye morphology; Northern elephant seals; vision; anatomy; scotopic; retina; ganglion cells

INTRODUCTION

Northern elephant seals (NES) are pelagic northern Pacific seals. They are widely known as one of the deepest and longest diving pinnipeds by virtue of regularly reaching the aphotic or bathypelagic zone during their foraging dives (Delong and Stewart, 1991). Among all marine mammals, only some cetaceans, such as the sperm whale, can rival NES in this endeavor (Watwood et al., 2006; Debey and Pyenson, 2013). The only sources

Grant sponsor: Office of Associate Dean of Research, College of Veterinary Medicine, Western University of Health Sciences, Pomona, CA.

*Correspondence to: Hrvoje Smodlaka DVM, PhD, Western University of Health Sciences, College of Veterinary Medicine, 309 E. Second Street, Pomona, CA, 91766-1854, USA. E-mail: hsmodlaka@westernu.edu

Received 29 September 2014; Revised 22 January 2016; Accepted 12 February 2016.

DOI 10.1002/ar.23342

Published online 7 March 2016 in Wiley Online Library (wileyonlinelibrary.com).

of light in the deepest part of their foraging habitat are bioluminescent flashes of deep sea organisms, as downwelling surface light is attenuated before it reaches the bathypelagic zone (Warrant, 2004). The scarcity of light in deep sea environments imposes strong selection for high light sensitivity among all visual foragers that are active in this zone.

Physiological optics predicts several mechanisms to improve light sensitivity at the level of retinal fine structure and at the level of eye optics. Visual light sensitivity of the retina is improved by increasing the proportion of rods, which are more sensitive to light than cone photoreceptors (Warrant, 2004); sometimes, rod photoreceptors are stacked in multiple layers to increase the probability of photon capture (Locket, 1977; Martin et al., 2004). A different mechanism is accomplished by the tapetum lucidum, an iridescent segment of the choroid which reflects nonabsorbed photons back to the photoreceptor layer, effectively providing a second opportunity for photons to be captured. Another approach is to increase retinal summation, *i.e.*, connecting a high number of photoreceptors to only a few ganglion cells, resulting in higher action potential likelihood in the afferent optic axons (Land, 1981; Land 1990; Welsch et al., 2001; Land and Nilsson, 2012).

At the optical level, the diameter of the fully dilated pupil is a key variable in assessing the ability of an eye to collect light, regardless whether light is coming from an extended scene or from a point light source such as bioluminescence. Retinal illumination, a ratio considered to scale proportionally with the sensitivity to extended light sources, is improved by having a large pupil for a given posterior nodal distance (Hughes, 1977; Land, 1981; Motani et al., 1999; Warrant 1999; Warrant, 2004; Schmitz and Motani, 2010; Schmitz and Wainwright, 2011). The ability to detect point light sources is considered to increase with a larger pupil for given number of photoreceptors (Land, 1981; Warrant, 2004; Schmitz and Motani, 2010; Schmitz and Wainwright, 2011). Recent modeling efforts that account for both optics and retinal physiology have shown that absolutely large eyes are beneficial for multiple optical functions in the deep pelagic realm (Nilsson et al., 2012; Schmitz et al., 2013). Large eyes improve the detection of potential bioluminescent prey and predators of various sizes.

This introductory summary of visual performance illustrates that there are multiple potential mechanisms to enhance light sensitivity, but the current understanding of pinniped eye evolution in response to the dim photic environments of the deep sea is largely hindered by availability of data. While there is a fairly good understanding of the general features of pinniped eyes, the pattern of trait evolution remains poorly understood. Importantly, some existing hypotheses concerning the adaptive evolution of pinniped eye traits cannot be adequately tested without assessing additional species. Anatomical and histological data on NES are especially scarce. Given that NES regularly dive into the aphotic zone, indicating that their foraging niche extends much deeper than that of many other pinnipeds, additional visual modifications may be present.

The goal of this study is to carefully evaluate the anatomical and histological structure of NES eyes, and to assess the density and distribution of ganglion cells in the retina. Such data will be very valuable for future comparative analyses of the evolution and adaptive significance of visual performance features across marine mammals.

MATERIALS AND METHODS

The animals used for tissue sampling were obtained from the Marine Mammal Care Center at Fort MacArthur in San Pedro, CA. No animals were harmed or killed for the purpose of this project; all tissues were taken from animals that died naturally. All research activities were approved by the IACUC of Western University of Health Sciences (R09/IACUC/027) and the National Oceanic Atmospheric Administration (151408SWR2010PR00016:JGC).

Tissue samples were collected from a total of 10 NES (*Mirounga angustirostris*) weaners (6–11 months of age) ~30 min post mortem. Detailed gross anatomical dissections of the eye and eye adnexa were performed. Morphometric measurements of the eye globes were completed in both anterioposterior and mediolateral directions and the diameter of the cornea was also measured. Globes were injected with 2–3 ml of 10% neutral buffered formalin (NBF, pH7). Subsequently, the eye globes were submerged into the same 10% NBF. After fixation, histological tissue samples were excised from different segments of the eye (retina, sclera, cornea, choroid, lens, adnexa) and placed in fresh 10% NBF for further fixation. The eye tissue samples were cut into small sizes and processed with graded ethanol. In order to proceed with the paraffin embedding, ethanol in the tissue was replaced by xylene. The samples were then placed in melted paraffin to infiltrate the tissue. Tissue paraffin blocks were sectioned at 5 to 10 μm thickness, and the sections were mounted onto glass slides. Slides were selected for staining based on the quality of the tissue section (e.g., lack of knife marks, folds or tears). Sections of each tissue type were stained with Hematoxylin & Eosin and Masson's trichome stains to visualize tissue layers. A Nikon DS-5M camera mounted on a Nikon E600 microscope was used for photomicrography.

In order to assess ganglion cell topography and to prepare retinal wholemounts, eyes were injected with 2–3 ml 10% NBF, tagged with sutures for orientation, excised and submerged in NBF. Eye globes were transected vertically at the equator, creating two halves. The posterior half (containing the optic retina) was halved dorsoventrally, with vitreous body still attached. Retinal tissue was marked with tissue markers for orientation. The vitreous body was carefully removed with a small paintbrush. The optic nerve/disc was transected horizontally, thus freeing the retina. The retina was gently detached and floated onto a gelatinized slide, allowed to dry in formalin vapors overnight, and stained with cresyl violet solution (Harleco, EMD, Chemicals Inc. Gibbstown NJ 08027). Since the retinas were completely translucent, no prior manual removal of retinal pigment epithelium or bleaching techniques were necessary.

Ganglion cell densities were recorded using the stereological techniques designed for retinal wholemounts (Ullmann et al., 2012, Coimbra et al., 2013), using the optical fractionator module of Stereo Investigator 11 (MBF Bioscience). The samples were imaged with a QImaging 2000R camera connected to an Olympus BX61 microscope. The large size of the ganglion cells (on

average about 34 μm) and their sparse distribution required the use of the 10x/0.3 objective. First, the region of interest was defined by drawing contours around each retinal halve (see above paragraph), excluding the optic disc which featured thick nerve fibers. A sampling grid of 4,088 by 2,215 μm with a counting frame size of 250 by 250 μm was placed across both retinal halves, yielding a total of 300 sampling sites for dorsal and ventral partition combined. At each sampling site, the number of ganglion cells was counted following stereological principles (Coimbra et al., 2013). Although the cells of the retina were at different levels of focus in the wholemount, for the purpose of estimating cell population density, the retina was considered a single layer. Thus, when creating the settings for the Stereo Investigator program, the optical dissector height was defined so that all cells in the retinal ganglion cell layer (RGCL) were able to be counted. Great care was taken to fine-focus through the entire RGCL to ensure that no cells were missed. The following criteria (Coimbra et al., 2013) were used to identify ganglion cells: a) large polygonal soma, on average 6 times larger than any other cells in the retina b) dense Nissl substance staining c) eccentric, distinct, large nucleus and nucleolus present d) smaller, rounder cells with no Nissl stain were classified as amacrine cells; smaller rounder darkly stained cells we identified as glial cells; small elongated lightly stained cells were classified as endothelial cells- these cells were excluded from counting. We had two counters agreeing on every cell counted. The number of ganglion cells for each retinal half was estimated using the optical fractionator workflow of Stereo Investigator and summed to obtain an estimate for the whole retina. These estimates were only accepted after verifying that the Schmitz-Hof coefficient of error was less than 0.1.

The distribution of ganglion cells across the entire retina was visualized with the open-source tool "retina" (Cohn et al., 2015) developed for the statistical platform "R" (R Development Core Team, 2015). "Retina" formats the count data, retinal wholemount outline, and the optic disc outline and passes it on to "retistruct" (Sterratt et al., 2013) for a reconstruction of the hemispherical nature of the retinal cup, digitally stitching the incisions made for flattening the retinal tissue onto the microscope slide. Subsequently, "retina" produces an azimuthal equidistant projection of the data onto a flat surface and fits a thin plate spline smoothing function with the smoothing parameter lambda (set to 0.001 for NES count data). The coloration of each pixel in the projection represents the predicted retinal ganglion cell density from the spline function, and the x-marks in the reconstructed map show retinal locations where density was recorded. The thin plate spline function represents an objective representation of the count data and does not rely on manual interpolation (Cohn et al., 2015). The choice of lambda parameter will influence how closely the surface follows the actual counts. Very low lambda values tend to produce overfitted maps (low error at the sampling sites, but a warped appearance between sites), whereas high lambda values tend to deliver oversimplified maps. One can assess the model fit by investigating the frequency distribution of errors, which reveals by how much the fitted surface deviates from the actual counts at each of the sampling locations. Depending on the lambda settings, the absolute peaks are often conservatively estimated, especially if defined by a high count from a single sampling location. This means that the fitted surface, which is an estimate of the cell density, is lower than the absolute count value. The location of the peak is correctly indicated, but the surface fit has the desirable effect of erring on the cautious side when interpreting the highest densities, accounting for possible artifacts.

RESULTS

Gross anatomical observations

The average anteroposterior diameter (i.e., from cornea to sclera, measured along the optic axis) of the sampled eye globes was 4.4 cm (±0.2) (N = 6), while the average equatorial diameter was slightly larger (5.03 cm ± 0.25). The notably thin extraocular muscles (~1 mm) were attached to the globe just posterior to the equator and appeared nearly transparent. The optic nerve exited the ventrotemporal posterior aspect of the eyeball. The spherical lens had a diameter of 1.9 cm (N = 6).

Histological Findings: Fibrous Tunic

Sclera. The sclera was composed of dense collagenous connective tissue organized in laminar sheets that interdigitate longitudinally and circularly. Peripherally, the episclera consisted of loose connective tissue. The sclera was thick posteriorly and anteriorly (3.1 mm ± 0.45), providing strong mechanical support to the eye globe. However, the sclera was substantially thinner at the equator (0.4 mm ± 0.29), where the eyeball can easily be indented. Large arteries, veins and nerves perforated the sclera anteriorly. Venules and arterioles supplying and draining the sclera were observed in the periphery, while capillaries were present deeper in the scleral tissue. At the level of the optic disc, vascular plexuses perforated the sclera (together with the optic nerve), thus becoming incorporated into the vascular tunic.

Cornea. The diameter of the cornea reached 3.51 (±0.16) cm. The anterior epithelium of the cornea was a noncornified stratified squamous epithelium, with an anterior limiting membrane underneath. At the junction with the bulbar conjunctiva, the epithelium had a distinct layer of melanocytes deep to the basal lamina in the stratum basale. Melanosomes were observed deep among the epithelial cells. This region corresponds roughly to the position of the limbus corneus. The substantia propria featured straight, unidirectionally placed collagen fibers with scattered flattened fibroblasts. The posterior limiting membrane served as an attachment for the simple squamous posterior epithelium.

Histological Findings: Vascular Tunic

Choroid proper. The first layer (basal complex) was composed of endothelial cells attaching directly to the layer of pigmented epithelium of the retina. Its second layer was the chorio-capillary layer. Even though largely missing, some dispersed capillaries sporadically occur. Beneath, the tapetum lucidum covered nearly the entire fundus of the eye. The tapetum normally

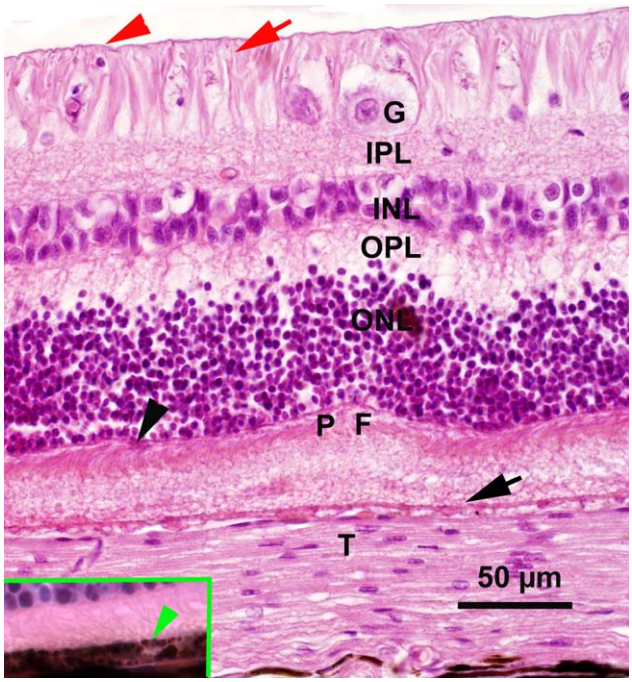

Fig. 1. Anterior portion of retina and choroid (closer to ora serrata). Hematoxylin and eosin stain. T, tapetum lucidum, arrowhead (black)-outer limiting membrane; P, photoreceptor layer; arrow (black), clear retinal pigmented epithelium, F-fold inside the retina; ONL, outer nuclear layer; OPL, outeplexiform layer; INL, inner nucler layer; IPL, inner plexiform layer; G, ganglion cell layer; arrow(red), optic nerve fiber layer; arrowhead (red), inner limiting membrane. Insert (at ora serrata); green arrowhead-pigments in pigmented retinal epithelium. Note the absence of tapetum lucidum cells underneath the epithelium.

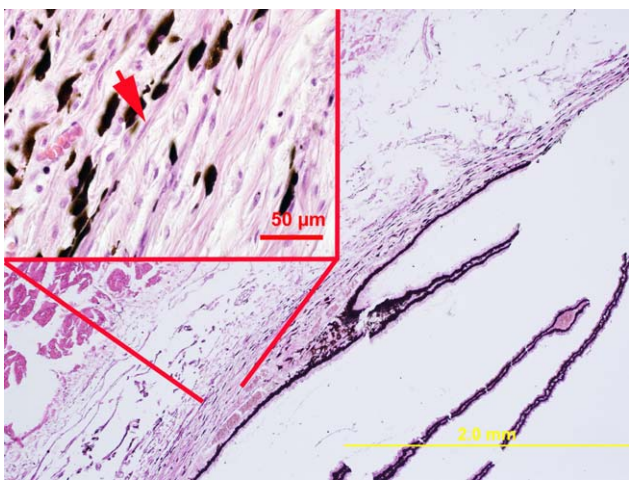

Fig. 2. Ciliary body, with ciliary processes. Hematoxylin and eosin stain. Right side of the image aims posteriorly and left side aims anteriorly. Insert: arrow-scattered strands of ciliary muscle.

consisted of 20–50 layers of rectangular cells (Fig. 1), but an increase in the number of cell layers in the posterior regions (40–50) resulted in a maximum tapetal thickness of 130.5 ± 17 µm. Closer to the ora serrata, the tapetum lucidum dramatically decreased in thickness to

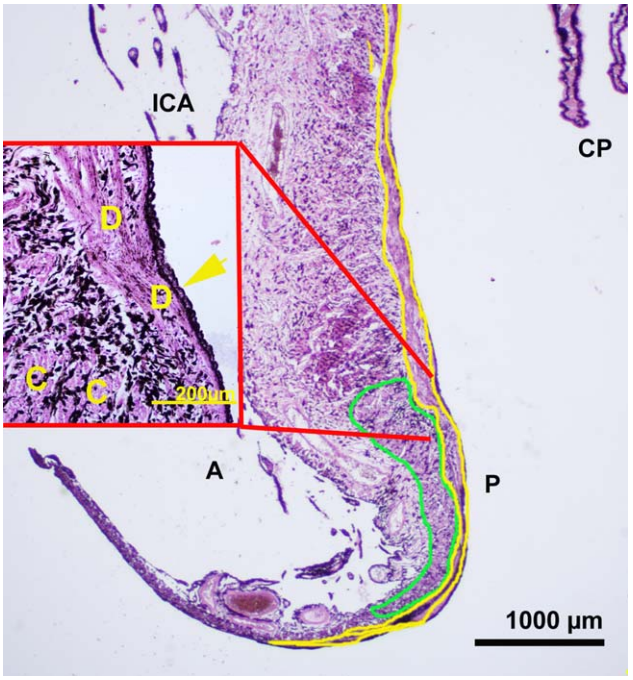

Fig. 3. Iris, longitudinal section. Hematoxylin and eosin stain. Area outlined in green -constrictor of the pupil, Area outlined in yellow- dilator of the pupil, A-anterior surface, P-posterior surface, ICA-iridocorneal angle, CP-ciliary processes. Insert: arrow-posterior epithelium, C-constrictor pupillae m., D-dilator pupillae m.

1–2 cell layers and eventually disappeared. The vascular layer of the choroid was predominantly composed of large diameter veins, along with smaller arteries, venules, and arterioles. The loose connective tissue displayed many granules containing melanin, whereas the suprachoroid layer mainly contained thin collagen bundles with a few dispersed fibroblasts.

Ciliary body. The bulk of the ciliary body was composed of loose collagenous connective tissue, rich in capillaries, melanocytes and discontinuous bundles of poorly developed smooth ciliary muscle (Fig. 2). Posteriorly, the ciliary body was covered by two epithelial layers, a heavily pigmented cuboidal epithelium and a deeper layer of non-neural columnar cells (ciliary epithelium), which together constituted the pars ciliaris retinae. Ciliary processes were elongated and entirely covered by the bi-layered cuboidal epithelium. Deep to the epithelium of the ciliary processes was a meshwork of capillaries, venules, arterioles, and veins.

Iris. The anterior surface and the iridal stroma were composed of collagenous connective tissue, capillaries, venules and dispersed melanocytes (Fig. 3); autonomic nerve fibers were observed infrequently. Posterior to the stroma was a layer of organized smooth muscle cells. The perpendicularly oriented dilator pupillae muscle originated from the base of the iris and continued towards its free edge, whereas, the more circularly oriented constrictor pupillae was closer to the free edge of the pupil (Fig. 3). The constrictor pupillae was more anteriorly located in respect to the dilator pupillae (Fig.

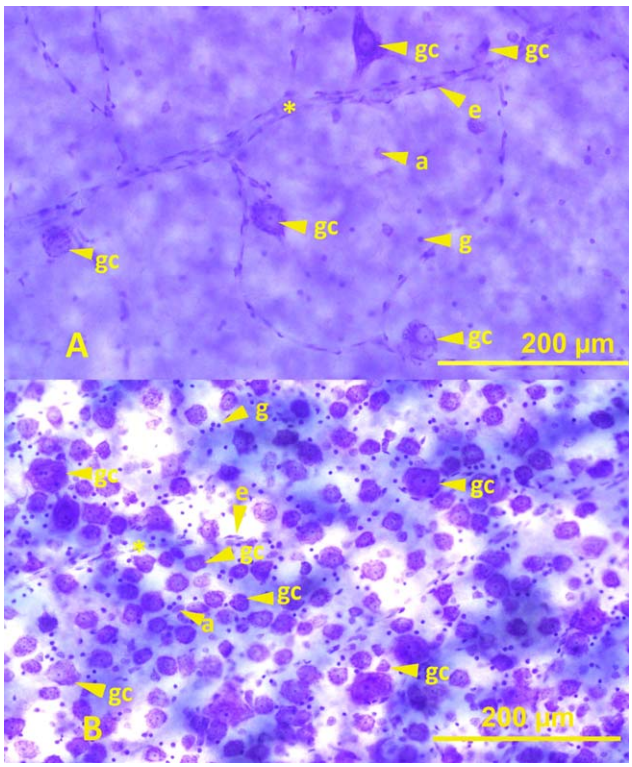

Fig. 4. Retinal wholemount; two different areas showing ganglion cells in sparse (**A**) and dense regions (**B**). Cresyl violet stain. Asterisk-vessel, a-amacrine cells, gc-ganglion cells, e-endothelial cells, g-glial cells. The count of ganglion cells in the area of 4B was determined, after focusing through the entire layer, to be 193.

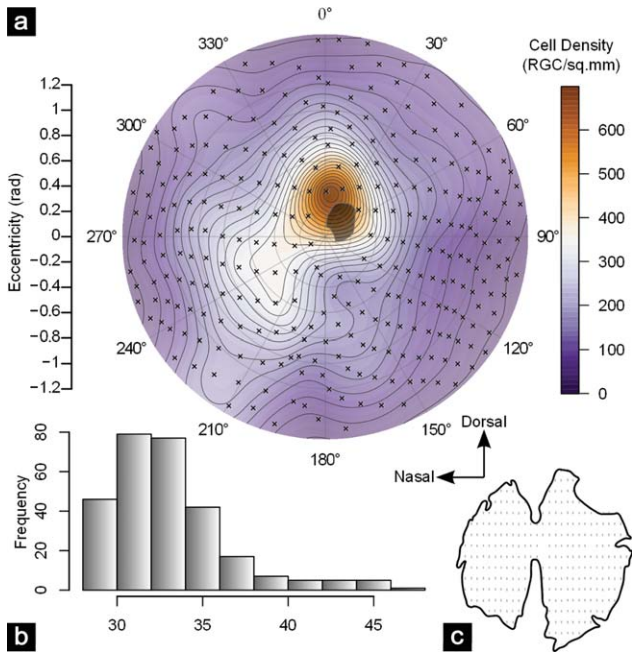

Fig. 5. (a) Retinal ganglion cell layer (RGCL) topography of the northern elephant seal (*Mirounga angustirostris)*, visualized with the R package *retina* (Cohn et al., 2015). The color gradient represents the interpolated cell density retrieved from a thin plate spline smoothing function. The smoothing parameter lambda was set to 0.001, along with a second-order polynomial. Frequency distributions of the model error, that is, the difference between true and predicted cell density at each sampling site are displayed in (**b**). The original outline of the retinal wholemount and the locations of all sampling sites are illustrated in (**c**).

3). Myocytes of the dilator pupillae were heavily pigmented (Fig. 3). Finally, the pars iridica retinae was composed of pigmented epithelium and nonpigmented epithelium (Fig. 3).

Iridocorneal angle. The pectinate ligaments delimited the iridocorneal angle superficially and were studded with occasional capillaries and venules. Endothelial cells coated the pectinate ligaments externally (Fig. 3). Deep to the pectinate ligaments was a trabecular meshwork with venous plexuses.

Histological Findings: Nervous Tunic

Retina. The pars optica retinae was composed of 10 distinct retinal layers (Fig. 1), averaging 205.8 ± 24 µm in complete thickness. The most peripheral layer was made of pigmented epithelium. Despite the name of this tissue layer, most of its cells were in fact non-pigmented in NES (Fig. 1), except in the area close to the ora serrata. Photoreceptors, mainly densely packed rods, were found directly beneath the epithelial layer. However, cone photoreceptors were also observed. Sometimes the photoreceptor layer appeared folded (Fig. 1), but the folds gradually disappeared towards the ora serrata. Sometimes the folding was observed in outer nuclear layer (up to 20 nuclei thick) and outer plexiform layer. The inner nuclear layer was composed of 1-5 layers of bipolar neurons (Fig. 1) along with the amacrine and horizontal cells. The RGCL was formed by a single stratum of ganglion cells (Fig. 1), which at the ora serrata became difficult to discern due to scarcity of cells. Ganglion cells averaged 34 ± 11 µm in diameter across the entire retina ($N = 33$, range 17–61 µm).

The RGCL contained an estimated 377,000 cells across the entire retina. The Schmitz-Hof coefficient of error was <0.1 for both halves of the retina (0.085 and 0.084, respectively), and the thin plate spline interpolation used for map visualization matches the sampled data ($R^2 = 0.808$). Ganglion cells were very sparse (Fig. 4A) closer to the ora serrata (less than 100 cells per mm^2) but their density increased (Fig. 4B) towards the optic disc (Fig. 5). The absolute maximum density of 1,312 cells per mm^2 was reached immediately dorsal to the optic disc. The ventral half of the retina featured moderately high cell densities, especially in a broad ridge that extends nasoventrally.

The optic nerve fiber layer of the retina was well developed and reached its maximum thickness near the optic disc. The optic nerve at this point was surrounded by a prominent vascular plexus.

DISCUSSION

The detailed description of gross morphology and histology of NES eyes provides a wealth of information for a better understanding of the potential evolutionary

adaptations to deep-sea photic environments. While some of the features described in this study substantiate previous findings regarding pinniped eye morphology and histology, several important observations expand the current knowledge, indicating possibly unique traits of NES.

In agreement with the literature on pinnipeds, NES eyes are large, in both absolute and relative terms (Jamieson and Fisher, 1972; Welsch et al., 2001; Mass and Supin, 2007; Debey and Pyenson, 2013), feature a spherical lens (Pütter, 1903; Welsch et al., 2001; Mass, 2009), a thickened anterior and posterior sclera (Pütter, 1903), and possess a photoreceptor layer largely consisting of rods (Peichl and Moutairou, 1997; Peichl et al., 2001; Griebel et al., 2006).

The presence of well-developed pupillary constrictor and dilator muscles in NES eyes indicates a powerful ability to regulate pupillary diameter. Indeed, a large range of pupillary constriction and dilation has been described in NES, harbor and Weddell seals (Jamieson and Fisher, 1972; Levenson and Schusterman, 1997; Welsch et al., 2001; Mass and Supin, 2007; Hanke et al., 2009a). In contrast, the ciliary muscle of NES is weakly developed, similar to Weddell (Welsch et al., 2001) and southern elephant seals (Pütter, 1903). Relatively weak ciliary muscle, coupled with a spherical lens, suggests a slight range of lens accommodation, which is congruent with the observations in harbor seals (Hanke et al., 2006). Amphibious birds and deep-sea fishes also have spherical lenses; however, birds carry well developed ciliary muscle (Sivak et al., 1985) and fishes carry a specialized lens muscle (Kikuchi et al., 1994) which enables their accommodation. Given the almost perfectly spherical shape of the lens, NES are likely emmetropic in water and myopic in air. However, it is possible that constricting the pupil to a small vertical slit or even pinhole in combination with flattened corneal topography mitigates the effects of aerial myopia in a similar way to what has been documented for harbor seals (Hanke et al., 2006). NES have the largest pupillary area (422.3 mm^2) among pinnipeds, which can constrict to just 0.9 mm^2 (Levenson and Schusterman, 1997). In addition, NES have the largest range of pupillary area (469.2) when compared to the shallow diving pinnipeds (Levenson and Schusterman, 1997).

The large extent of the tapetum lucidum is a hallmark characteristic of pinniped eyes that has been documented in harbor seals (Johnson, 1901; Jamieson and Fisher, 1972), Weddell seals (Welsch et al., 2001), Steller's sea lions (Mass, 2004), Caspian seals (Mass, 2009) and California sea lions (Miller et al., 2010). In NES a grayish-blue tapetum lines the entire eye fundus and only dissipates close to the ora serrata, whereas the metallic blue-green tapetum of domestic mammals is restricted to the region dorsal to the optic disc (Dyce et al., 1996). A tapetum lining the whole fundus assures that the beneficial effects of improved photon collection are provided across the entire visual field of an animal which is active in three-dimensional aquatic environments (Ollivier et al., 2004).

Pinnipeds are considered to have the thickest tapetum lucidum among vertebrates (Walls, 1942). Weddell seals (30 cell layers thick; Welsch et al., 2001) and harp seals (34 cells; Nagy and Roland, 1970) feature very prominent tapeta, yet the tapetum of NES is even thicker. The tapetum lucidum of NES carries up to 50 cell layers and is 130.5 ± 17 μm thick in the posterior part of the eye, which equals 63% of the retinal thickness. A thicker tapetum may potentially provide more reflectance and thus improve photon capture in scotopic environments.

The retina of NES features a remarkable folding within the photoreceptor and outer nuclear layer, which was first shown by Landau and Dawson (1970). Folding of some retinal layers has been described previously in harbor seals (Jamieson, 1970; Jamieson and Fisher, 1971), sperm whales (Mann, 1946), megachiroptean bats (Pedler and Tilley, 1969; Fejér et al., 2001), hippopotamus, beluga whales and European river otters (Pilleri, 1967) and escolar (Landgren et al., 2014). We cannot fully exclude that the folding is an artifact, but given that folding occurred in multiple NES specimens it is likely real. Pilleri (1967) postulated convergent evolution of retinal folding in adaptation to aquatic habitats, though folds were also described in the retina of megachiropteran bats. Fejér et al. (2001) suggested that retinal folds may have photometric function in fruit bats, albeit this hypothesis remains untested.

The peak ganglion cell density within the RGCL of NES (1,300 cells/mm^2) falls into the lower range for pinnipeds described so far (1,250–3,952 cells/mm^2; Welsch et al., 2001; Mass and Supin, 2003; Mass, 2004; Mass, 1992; Hanke et al., 2009b; Mass, 2009). Only the walrus features lower densities of ganglion cells (1,250 cells/mm^2; Mass, 1992) than NES. Much lower estimates of ganglion cell densities (65 cells/mm^2) have been reported for adult deep-diving southern elephant seals (Pütter, 1903), although it should be noted that these numbers were derived by methods not meeting current standards. The density was derived from an average distance between ganglion cells and not actual counting following stereological principles. Also, there is no information on how many inter-ganglion cell distances were measured and at what location in the retina; hence, we question Pütter's (1903) data.

Low densities of retinal ganglion cells are frequently observed in scotopic vertebrates and are often a sign of high convergence of photoreceptors on ganglion cells. Landau and Dawson (1970) estimated the photoreceptor to ganglion cell ratio to be at 800:1 in NES, and the low peak density that we documented in this study is compatible with this estimate. Most other pinnipeds that have been evaluated so far have higher ganglion cell densities than NES, which may indicate less dramatic convergence of photoreceptors to ganglion cells. Given that many of the pinniped species, listed above, do not routinely reach depths as extreme as the NES (Debey and Pyenson, 2013), their higher ganglion cell densities seem sensible.

An interesting pattern was observed concerning retinal cell topography. Nearly all investigations in pinnipeds have found areas of high ganglion cell density dorsolateral to the optic disc in the temporal quadrant (Welsch et al., 2001; Mass and Supin, 2003; Mass and Supin, 2007; Mass, 2009). NES also exhibits a densest zone dorsal to the optic disc, but in addition presents with slightly elevated cell densities in the ventronasal half of the retina. This is somewhat similar to escolars, predatory deep-sea fish with ganglion cell density peaks in both dorsal and ventral halves (Landgren et al., 2014). Landgren et al. (2014) proposed that the ventral

peak may be responsible for viewing the silhouette of prey swimming above, while the temporal peak may aid in viewing prey swimming in front of the predator. It is possible that the slightly elevated ganglion cell count in the ventral region of NES retina has a similar function as the ventral peak in escolars, indicating emerging, or imperfect convergence.

In conclusion, our careful anatomical and histological eye evaluation reveals that the morphology of NES eyes conforms well to the general anatomy of other pinnipeds. NES present a trait syndrome that is fully consistent with evolutionary adaptations to aquatic dim light conditions, including ocular size, lens shape, scleral thickness, and rod-dominance. The dilator and constrictor pupillae muscles are well developed, indicating an excellent dark/light adaptation capability. On the other hand, weakly developed ciliary muscle suggests minimal lenticular accommodation. Ganglion cell densities are low, suggesting a high degree of retinal summation resulting in improved light sensitivity, and yet lower visual acuity. Additional observations enrich the understanding of pinniped eye morphology and its potentially adaptive significance, in particular the large extent and the exceptional thickness of the tapetum lucidum. The peculiar folding of the retinal layers is currently without functional interpretation, even though it may be related to dim light environments. Our data on NES will provide an important resource for analyses of the evolutionary processes that lead to the trait complex seen in extreme divers.

ACKNOWLEDGEMENTS

The United States Department of Commerce, National Oceanic and Atmospheric Administration, National Marine Fisheries Services granted access to seal specimens used in this study (Permit #151408SWR2010PR00016:JGC).

LITERATURE CITED

Cohn BA, Collin SP, Wainwright PC, Schmitz L. 2015. Retinal topography maps in R: new tools for the analysis and visualization of spatial retinal data. J Vison 15:19. doi:10.1167/15.9.

Coimbra PC, Hart NS, Collin SP, Manger PR. 2013. Scene from above: retinal ganglion cell topography and spatial resolving power in the giraffe (Giraffa camelopardis). J Comp Neurol 521: 2042–2057.

Debey LB, Pyenson ND. 2013. Osteological correlates and phylogenetic analysis of deep diving in living and extinct pinnipeds: what good are big eyes? Mar Mamm Sci 29:48–83.

Delong RL, Stewart BS. 1991. Diving patterns of northern elephant seal bulls. Mar Mammal Sci 7:369–384.

Dyce KM, Sack WO, Wensing CGG. 1996. Textbook of veterinary anatomy. 2nd ed. St. Louis: W.B. Saunders Company.

Fejér Z, Haldar C, Ghosh M, Frank LC, Szepessy Z, Szél A, Manzano e silva MJ, Vigh B. 2001. Pineal organ-like organization of the retina in megachiroptean bats. Acta Biol Hung 52:17–27.

Hanke FD, Dehnhardt G, Schaeffel F, Hanke W. 2006. Corneal topography, refractive state, and accommodation in harbor seals (*Phoca vitulina)*. Vis Res 46:837–847.

Hanke F, Hanke W, Scholtyssek C, Dehnhardt G. 2009a. Basic mechanisms in pinniped vision. Exp Brain Res 199:299–311.

Hanke FD, Peichle L, Dehnhardt G. 2009b. Retinal ganglion cell topography in juvenile harbor seals (*Phoca vitulina*). Brain Behav E 74:102–109.

Hughes A. 1977. The topography of vision in mammals of contrasting life style: comparative optics and retinal organization. In: Crescitelli F. editor. The visual system in vertebrates. Springer-Verlag Berlin: Heidelberg. p 613–756.

Jamieson GS. 1970. The eye of the harbour seal, *Phoca Vitulina*. Masters Thesis The University of British Columbia: Vancouver.

Jamieson GS, Fisher D. 1971. The retina of the harbour seal, *Phoca vitulina*. Can J Zool 49:19–23.

Jamieson GS, Fisher D. 1972.The pinniped eye: a review. In: Harrison RJ, editor. Functional anatomy of marine mammals. London: Academic Press. p 245–261.

Johnson GL. 1901. Contributions to the comparative anatomy of the mammalian eye, chiefly based on ophthalmoscopic examination. Philos Trans R Soc B 194:1–84.

Kikuchi K, Asai M, Kuboshima Y, Mitani I, Takizawa T, Okiyama M, Somiya H. 1994. Visual accommodation system in the eyes of a berycid deep-sea fish beryx splendens. Fish Sci 260:691–694.

Land MF.1981. Optics and vision in invertebrates. In: Land MF, Laughlin SB, Nässel DR, Strausfeld NJ, Waterman TH. editors. Comparative physiology and evolution of vision in invertebrates. B: Invertebrate visual centers and behavior I. Springer–Verlag: Berlin, Heidelberg, New York. p 471–592.

Land MF. 1990. Optics of the eyes in marine animals. In: Herring JP, Campbell AK, Maddock L, editors. Light and life in the sea. Cambridge: Cambridge University Press. p 149–166.

Land MF, Nilsson DE. 2012. Animal eyes. 2nd ed. Oxford: Oxford University Press.

Landgren E, Fritsches K, Brill R, Warrant E. 2014. The visual ecology of a deep-sea fish, the escolar *Lepidocybium flavobrunneum* (Smith, 1843). Philos Trans R Soc Lond B Biol Sci 6:369.

Landau D, Dawson WW. 1970. The histology of retinas from Pinnipedia. Vis Res 10:691–702.

Levenson DH, Schusterman RJ. 1997. Pupillometry in seals and sea lions, ecological implications. Can J Zool 75:2050–2057.

Locket NA. 1977. Adaptations to the deep-sea environment. In: Crescitelli F, editor. Handbook of sensory physiology, vol VII/5. Springer: Berlin Heidelberg, New York. p 67–192.

Mann G. 1946. Oyo y vision de las ballenas. Biologica 4:23–71.

Martin G, Rojas LM, Ram Y, McNeil R. 2004. The eyes of oilbirds (*Steatornis caripensis*): pushing at the limits of sensitivity. Naturwissenschaften 91:26–29.

Mass AM. 1992. Retinal topography in walrus (*Odobenus rosmarus diverges*) and fur seal (*Callorhinus ursinus*). In: Thomas JA, Kastelein RA, Supin AY, editors. Marine mammal sensory syetem. New York: Plenum. p 119–135.

Mass AM, Supin AY. 2003. Retinal topography of the Harp Seal *Pagophylus groenlandicus*. Brain Behav E 62:212–222.

Mass AM. 2004. A high-resolution area in the retinal ganglion cell layer of the Steller's sea lion (*Eumetopias jubatus*): a topographic study. Dokl Biol Sci 396:187–190.

Mass AM, Supin A. 2007. Adaptive features of aquatic mammals' eye. Anat Rec 290:701–715.

Mass AM. 2009. Localization of the highest retinal resolution area in the retinal ganglion cell layer of the Caspian seal phoca caspica: a topographic study. Dokl Biol Sci 429:575–578.

Miller S, Colitz C, Dubielzig R. 2010. Anatomy of the California sea lion globe. Vet Ophthalmol 13:63–71.

Motani R, Rothschild BM, Wahl W, Jr. 1999. Large eyballs in diving ichthyosaurs. Nature 402:747.

Nagy AR, Ronald K. 1970. The harp seal, *Pahophylus groenlandicus* (Erxleben, 1777). VI. Structure of retina. Can J Zool 48:367–370.

Nilsson D-E, Warrant EJ, Johnsen S, Hanlon R, Shashar N. 2012. A unique advantage for giant eyes in giant squid. Curr Biol 22:1–6.

Ollivier FJ, Samuelson DA, Brooks DE, Lewis PA, Kallberg ME, Komáromy AM. 2004. Comparative morphology of the tapetum lucidum (among selected species). Vet Ophthalmol 7:11–22.

Pedler C, Tilley R. 1969. The retina of a fruit bat (*Pteropus giganteus* Brünnich). Vis Res 9:909–922.

Peichl L, Moutairou K. 1997. Absence of blue cones in the retinae of some mammals. Inves Ophth Vis Sci 38:331–331.

Peichl L, Berhmann G, Kröger RHH. 2001. For whales and seals the ocean is not blue: a visual pigment loss in marine mammals. Eur J Neurosci 13:1520–1528.

Pütter A. 1903. Die Augen der Wassersäugethiere. Zool Jahrb 17:97–402.

Pilleri G. 1967. Retinalfalten im Auge von Wassersäugetieren. Experientia 23:54–55.

R Core Team. 2015. R: A language and environment for statistical computing. R Foundation for Statistical Computing, Vienna, Austria. Available at: http://www.R-project.org/.

Schmitz L, Motani R. 2010. Morphological differences between the eyeballs of nocturnal and diurnal amniotes revisited from optical perspectives of visual environments. Vis Res 50:936–946.

Schmitz L, Wainwright PC. 2011. Nocturnality constrains morphological and functional diversity in the eyes of reef fishes. BMC Evol Biol 11:338.

Schmitz L, Motani R, Oufiero CE, Martin CH, McGee MD, Gamarra AR, Lee JJ, Wainwright PC. 2013. Allometry indicates giant eyes of giant squid are not exceptional. BMC Evol Biol 13:45.

Sivak JG, Hildebrand T, Lebert C. 1985. Magnitude and rate of accommodation in diving and nondiving birds. Vision Res 25:925–933.

Sterratt DC, Lyngholm D, Willshaw DJ, Thompson ID. 2013. Standard anatomical and visual space for the mouse retina: computational reconstruction and transformation of flattened retinae with the Retistruct package. PLoS Computat Biol 9:e1002921.

Ullmann JFP, Moore BA, Temple SE, Fernández-Juricic E, Collin SP. 2012. The retinal wholemount technique: a window to understanding the brain and behaviour. Brain Behav E 79:26–44.

Walls GL. 1942. The vertebrate eye and its adaptive radiation. New York: Hafner Press.

Warrant EJ. 1999. Seeing better at night: life style, eye design and optimal strategy of spatial and temporal summation. Vis Res 39: 1611–1630.

Warrant EJ. 2004. Vison in dimmest habitats on earth. J Comp Physiol 190:765–789.

Watwood SL, Miller PJO, Johnson M, Madsen PT, Tyack PL. 2006. Deep-diving foraging behavior of sperm whales (Phylseter macrocephalus). J Anim Behav 75:814–825.

Welsch U, Ramdohr S, Riedelscheimer B, Hebel R, Eisert R, Plötz J. 2001. Microscopic anatomy of the eye of the deep diving Antarctic Weddell seal. J Morphol 248:165–174.